Crystal Structure, Polymorphism, and Properties of the New Vanadyl Phosphate $Na_4VO(PO_4)_2$

Rodion V. Panin, Roman V. Shpanchenko,* Andrei V. Mironov, Yuri A. Velikodny, and Evgeny V. Antipov

Department of Chemistry, Moscow State University, 119992 Moscow, Russia

Joke Hadermann

EMAT University of Antwerp (RUCA), Groenenborgerlaan 171, 2020 Antwerp, Belgium

Vasily A. Tarnopolsky and Andrei B. Yaroslavtsev

Kurnakov Institute of General and Inorganic Chemistry RAS, 119991, Leninsky pr. 31, Moscow, Russia

Enrique E. Kaul and Christoph Geibel

Max-Plank Institute CPfS Nöthnitzer Str. 40, 01187 Dresden, Germany

Received November 11, 2003. Revised Manuscript Received December 23, 2003

The new vanadyl phosphate $Na_4VO(PO_4)_2$ was synthesized and investigated by X-ray powder and single-crystal diffraction, high-temperature X-ray diffraction, electron diffraction, high-resolution electron microscopy, thermal analysis, magnetic susceptibility, and conductivity measurements. The compound undergoes a reversible phase transition at about 200 °C. The crystal structure of low-temperature β-$Na_4VO(PO_4)_2$ was solved using X-ray single-crystal data. This phase has an orthorhombic unit cell with lattice parameters $a = 16.0068(12)$ Å, $b = 14.5129(8)$ Å, $c = 7.0231(5)$ Å, S.G. *Pbca*, and $Z = 8$. The crystal structure of β-$Na_4VO(PO_4)_2$ is built by isolated chains formed by corner-shared $V^{4+}O_6$ octahedra linked additionally via corners by two PO_4 tetrahedra. All chains in the structure are equivalent. Na cations are located between the chains in an ordered manner. High-temperature α-$Na_4VO(PO_4)_2$ also has an orthorhombic cell with lattice parameters $a = 15.595(1)$ Å, $b = 14.651(2)$ Å, $c = 7.0262(6)$ Å, S.G. *Ibam*, and $Z = 8$. Electron diffraction study revealed an existence of various structural transformations occurring in situ in the transmission electron microscope. In both α- and β-modifications, the susceptibility follows a Curie−Weiss law with a very small Curie−Weiss temperature, indicating a very weak magnetic exchange among the V^{4+} ions.

Introduction

Reduced V-based mixed oxides with low-dimensional structures often exhibit unusual magnetic behavior. This makes them very attractive objects for investigators. Vanadium in oxidation states <+5 may adopt different coordination arrangement and form structures containing chains, ribbons, or layers formed by VO_n polyhedra. These low-dimensional fragments may be linked with each other by polyhedra containing a nonmagnetic cation (for instance, $P^{5+}O_4$ or $V^{5+}O_4$ tetrahedra), resulting in a two- or three-dimensional framework.

A chain of corner-shared VO_6 octahedra is one of the simplest structural units in low-dimensional structures. Some vanadyl(IV) orthophosphates of alkali metals contain chains in their structures. So in the α- and β-$LiVOPO_4$ structure,[1,2] chains of corner-shared octahedra exist. These chains are linked by PO_4 tetrahedra in a three-dimensional framework. α- and β-forms are distinguished by a tilt of octahedra and, correspondingly, phosphate groups. An antiferromagnetic transition at 40 K was found for the β-modification. A similar structure was found for $NaVOPO_4$,[3] which reveals an antiferromagnetic transition at 20 K. In the $KVOPO_4$ structure[4] VO_6 octahedra also form zigzag-like chains. The short vanadyl bond in all these structures is directed along the chains.

V^{4+}- and Ti^{4+}-containing complex phosphates often have similar structures due to the close crystallochemical characteristics of these cations. Both of them may adopt octahedral coordination with similar M−O bond lengths. These cations may form multiple vanadyl or

* To whom correspondence should be addressed. E-mail: shpanchenko@icr.chem.msu.ru.

(1) Lavrov, A. V.; Nikolaev, V. P.; Sadikov, G. G.; Poray-Koshitz, M. A. *Dokl. Akad. Nauk SSSR (Russ.)* **1982**, *266*, 343.
(2) Lii, K. H.; Li, C. H.; Cheng, C. Y.; Wang, S. L. *J. Solid State Chem.* **1991**, *95*, 352.
(3) Lii, K. H.; Li, C. H.; Cheng, C. Y.; Wang, S. L. *Z. Kristallogr.* **1991**, *197*, 67.
(4) Phillips, M. L. F.; Harrison, W. T. A.; Gier, T. E.; Stucky, G. D.; Kulkarni, G. V.; Burdett, J. K. *Inorg. Chem.* **1990**, *29*, 2158.

10.1021/cm0351543 CCC: $27.50
Published on Web 02/10/2004

titanyl bonds. For instance, crystal structures of the $M^IM^{IV}O(PO_4)$ (M^I = Li, Na; M^{IV} = V, Ti) have similar chainlike structures.[5−7] A shift of the cation out of the equatorial plane of the octahedra results in a short M^{IV}−O bond (≈1.6−1.7 Å). Simultaneously, the distance to the opposite oxygen atom is increased up to ≈2.1−2.4 Å. However, titanium often keeps regular octahedral coordination with equivalent bond lengths while for the V^{4+} cation a regular octahedral coordination is not typical. In the structure of titanyl(IV) phosphate $Na_4(TiO)(PO_4)_2$[8] infinite isolated chains of corner-shared TiO_6 octahedra exist and Na atoms are situated between these chains. This compound has a few polymorph modifications with different distribution of sodium atoms in the cell. In the high-temperature modifications, which are known as superionic conductors, sodium atoms randomly occupy positions between the chains, resulting in a high mobility of the cations.[9] At low temperature the structure becomes completely ordered, leading to successive commensurate and incommensurate modulated structures.[10−12]

Although $Na_4TiO(PO4)_2$ was reported a rather long time ago, no vanadyl(IV) phosphates with the same stoichiometry were found until now for any alkali metals. Below, we present the results of the synthesis and investigation of the new complex vanadyl phosphate $Na_4VO(PO_4)_2$ by X-ray diffraction at room and high temperatures, electron diffraction techniques, thermal analysis, conductivity, and magnetic properties measurements.

Experimental Section

$Na_4P_2O_7$ and VO_2 were used as initial reagents for the synthesis of $Na_4VO(PO_4)_2$. $Na_4P_2O_7$ was obtained by decomposition of Na_2HPO_4 at 700 °C. VO_2 was synthesized from V_2O_3 and V_2O_5 by annealing at 800 °C for 1 day in an evacuated and sealed quartz tube.

Green single-phase powder of $Na_4VO(PO_4)_2$ was synthesized by a solid-state reaction between stoichiometric mixture $Na_4P_2O_7$ and VO_2 (in molar ratio 1:1) in evacuated and sealed quartz ampules by annealing at 700 °C for 3 days followed by furnace cooling. Single crystals for structure analysis were obtained in an evacuated and sealed quartz tube by melting an as-prepared powder sample at 730 °C with subsequent furnace cooling.

X-ray powder diffraction (XPD) data were collected on a STOE diffractometer (Cu $K\alpha_1$ radiation, Ge monochromator, linear PSD). A high-temperature powder diffraction experiment was performed with the Guinier-Lenne camera (Cu Kα radiation, SiO_2 monochromator). Data collection for single-crystal structure refinement was done using a CAD4 diffractometer. Structure computations with the starting model were carried out using the CSD program package.[13] The final refinement was made with a JANA2000 program package.[14]

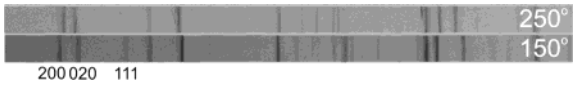

Figure 1. High-temperature XRD patterns of $Na_4VO(PO_4)_2$ taken in a Guinier-Lenne camera at 150 and 250 °C.

Thermal analysis was performed on a NETZSCH STA 449C instrument in purified Ar flow.

Ionic conductivity was measured by impedance spectrometry with the use of an impedance analyzer IPU-P.69 with a frequency range of 10 Hz to 2 MHz in air. The ac measurements were performed at cooling from 660 K to room temperature at water vapor pressure equal to 1800 Pa. The shape of an impedance plot was a semicircle starting at zero point. The conductivity value was obtained as an arc extrapolation to the real axis on the low-frequency side.

Electron diffraction (ED) at room and elevated temperatures and EDX analysis were performed on a Philips CM 20 microscope with a LINK-2000 attachment.

Magnetic susceptibility measurements were performed on a Quantum Design MPMS SQUID magnetometer in the range between 2 and 400 K at fields of 0.1, 1, and 5 T.

Results and Discussion

Synthesis and Polymorphism. X-ray powder pattern of the single-phase $Na_4VO(PO_4)_2$ sample was indexed in an orthorhombic unit cell with lattice parameters a = 15.9975(9) Å, b = 14.5041(12) Å, c = 7.0181(5) Å, and Z = 8. These parameters are close to those for the high-temperature form of the $Na_4TiO(PO_4)_2$ titanyl phosphate (a = 15.647 Å, b = 14.989 Å, c = 7.081 Å, S.G. *Ibam*). However, in contrast to the Ti-containing compound, strong peaks (for instance, ⟨111⟩: 19% or ⟨122⟩: 13%) corresponding to a primitive unit cell were present.

X-ray patterns of the $Na_4VO(PO_4)_2$ samples obtained by quenching ampules into water from different temperatures (300−700 °C) revealed an existence of a phase transition for $Na_4VO(PO_4)_2$. Quenching into water is the most convenient technique for obtaining a high-temperature form whereas quenching in air always resulted in a two-phase mixture. The XPD pattern of high-temperature α-$Na_4VO(PO_4)_2$ quenched from 450 °C was indexed in an orthorhombic symmetry with cell parameters a = 15.595(1) Å, b = 14.651(2) Å, c = 7.0262(6) Å, and Z = 8. Analysis of systematic extinctions allowed us to suppose the I-centered unit cell. In contrast to the bright-green low-temperature (β-) modification, the high-temperature (α-) form has grayish-green color. Despite very close cell parameters, two polymorphs are well-distinguished in the XPD patterns (Figure 1). The intensive 200 and 020 reflexes are the most informative for phase identification. Additionally, there is a strong 111 peak on the XPD pattern of the β-modification. A change of annealing conditions did not result in a change of the cell parameters for both modifications regardless of the presence (or not) of admixture phases.

Heating and cooling DTA curves for $Na_4VO(PO_4)_2$ are shown in Figure 2. Two clear peaks are seen in the heating curve of the β-$Na_4VO(PO_4)_2$ vanadyl phosphate

(5) Geifman, I. N.; Furmanova, N. G.; Nagornyi, P. G.; Li, D. Y.; Rotenfel′d, M. V. *Kristallografiya (Russ.)* **1993**, *38*, 88.
(6) Nagornyi, P. G.; Kapshuk, A. A.; Stus', N. V., Slobodyanik, N. S.; Chernega, A. N. *Zh. Neorg. Khim. (Russ.)* **1991**, *36*, 2766.
(7) Phillips, M. L. F.; Harrison, W. T. A.; Stucky, G. D.; McCarron, E. M.; Calabrese, J. C.; Gier, T. E. *Chem. Mater.* **1992**, *4*, 222.
(8) Maximov, B. A.; Klokova, N. E.; Verin, I. A.; Timofeeva, V. A. *Kristallografia (Russ.)* **1990**, *35*, 847.
(9) Klokova, N. E.; Maximov, B. A.; Tamazyan, R. A. *Kristallografia (Russ.)* **1993**, *38*, 56.
(10) Tamazyan, R. A., Maximov, B. A., Bolotina, N. B., Novikova, N. E.; Simanov, V. I. *Kristallografia (Russ.)* **1994**, *39*, 478.
(11) Bolotina, N. B.; Maximov, B. A.; Petricek, V.; Simanov, V. I. *Kristallografia (Russ.)* **1995**, *40*, 611.
(12) Maximov, B. A.; Bolotina, N. B.; Simonov, V. I.; Petricek, V.; Schulz, H. *Acta Crystallogr. B* **1994**, *50*, 261.
(13) Akselrud, L. G.; Zavalii, P. Yu.; Grin, Yu. N.; Pecharski, V. K.; Baumgartner, B.; Wölfel, E. *Mater. Sci. Forum* **1993**, *133−136*, 335.
(14) Petricek, V.; Dusek, M. *The crystallographic computing system JANA2000*; Institute of Physics: Praha, Czech Republic, 2000.

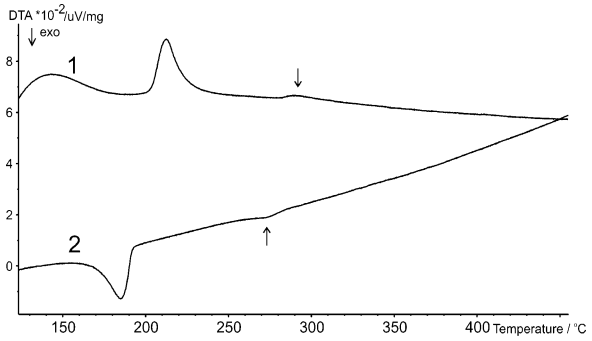

Figure 2. DTA curves for $Na_4VO(PO_4)_2$: 1, heating; 2, cooling.

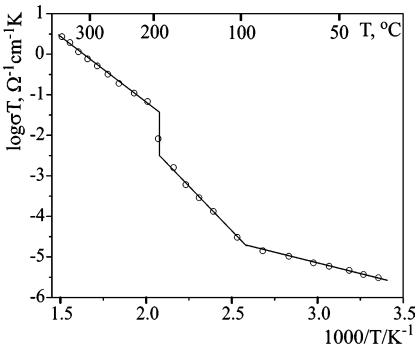

Figure 3. Temperature dependence of ionic conductivity for $Na_4VO(PO_4)_2$.

(curve 1). The first one at $T = 204$ °C is much stronger than the second peak at $T = 280$ °C. No further peaks were detected up to the melting point at 730 °C. At the cooling (curve 2), both peaks are also observed at 187 and 280 °C, respectively, indicating reversible transitions. The transition temperatures are well reproducible. At these conditions (temperature variation 5 K/min) the difference in the first transition temperature between heating and cooling is well-pronounced. It is kept at a temperature velocity of 1 K/min. In contrast to that the temperature of the second transition is the same for the cooling and heating regimes.

To clarify the results of the DTA measurements, additional high-temperature X-ray experiments were performed. Figure 1 shows the XPD patterns of $Na_4VO(PO_4)_2$ taken at 150 and 250 °C. After the cooling only reflexes corresponding to the low-temperature β-form were observed. Thus, the low-temperature transition corresponds to a reversible $\alpha \leftrightarrow \beta$ transformation. No visible changes were observed on the XPD patterns around 300 °C or upon heating to 700 °C. One may suggest that the weak second peak in the DTA curve corresponds to a minor structural transformation, which is not seen in the high-temperature experiment in the Guinier camera.

The temperature dependence of ionic conductivity (σ) for $Na_4VO(PO_4)_2$ ceramic sample is shown in Figure 3. At about 200 °C a conductivity jump (1 order of magnitude) is clearly seen on the $\sigma(T)$ plot. This jump corresponds to a phase transition revealed by DTA and XPD. Before and after the phase transition σ obeys an Arrhenius-type relationship ($\sigma(T) = \sigma_0 \exp(-E_a/kT)$) with activation energy 75 ± 6 and 56 ± 2 kJ/mol, respectively. Similar behavior of $\sigma(T)$ was found for $Na_4TiO(PO_4)_2$, which undergoes a phase transition at 262 °C.[15] A turning point at 100 °C may be attributed to a change of high-temperature self-defect conductivity with high activation energy to extrinsic conductivity with lower activation energy, for instance, to an occurrence of a minor quantity of V^{5+} or V^{3+} ions.[16] Since conductivity measurements were carried out in air, an additional DTA experiment was performed for $Na_4VO(PO_4)_2$. Heating of the sample in air up to 400 °C did not reveal an increase of mass that indicates the absence of vanadium atoms oxidation.

The quenching from 700 °C into water of an as-prepared sample of $Na_4VO(PO_4)_2$ revealed an existence of another modification with cell parameters of the orthorhombic unit cell $a = 15.444(3)$ Å, $b = 14.846(3)$ Å, $c = 7.007(1)$ Å, and $Z = 8$, having almost black color. The X-ray pattern of this form is very close to the α-form. Therefore, one may conclude that the crystal structures of both high-temperature forms should be very close. However, this form can be obtained by quenching after synthesis only and transforms irreversibly to α- or β-form after respective thermal cycling. We failed also to get this modification by heating of the β- or α-form up to the melting point followed by quenching. One may suggest that this polymorph is metastable and forms only during the synthesis.

Crystal structures for four polymorph modifications of $Na_4TiO(PO_4)_2$ were earlier described. In the low-temperature forms sodium atoms orderly occupy positions between the chains, whereas in the high-temperature phases Na positions are disordered and only partially filled. One might suspect that in the high-temperature polymorphs of the V-containing compound sodium atoms will also be disordered. This statement is supported by conductivity measurements. Except this, a comparison of the lattice parameters for these modifications indicates the disorder of sodium atoms at high temperatures. Obviously, the crystal structures of the high-temperature modifications are close to that for β-$Na_4VO(PO_4)_2$. This follows from the similarity of the cell parameters and X-ray patterns. However, contrary to expectations, the cell volume is reduced during the $\beta \rightarrow \alpha$ transition. This fact may be explained if one supposes that the sodium atoms, which are ordered between the chains in the β-phase (see below), become randomly distributed in different interstices in the α-structure. Such a distribution can be a reason for the shortening of the separation between the chains along the *a*-axes and consequently to a reduction of this parameter whereas the *b*-parameter is slightly increased. On the other side, the *c*-parameter is very slightly changed. This is also in agreement with our speculations since this parameter is determined only by the rigid geometry of the VO_6 chain where octahedra are cramped by PO_4 tetrahedra.

Crystal Structure of β-$Na_4VO(PO_4)_2$. The crystal structure of β-$Na_4VO(PO_4)_2$ was refined from single-crystal data. Since the cell parameters as well as the XPD pattern for $Na_4VO(PO_4)_2$ are very similar to those for the high-temperature modification of $Na_4TiO(PO_4)_2$,[8] this structure was taken as a model. Extinction conditions $hk0{:}h = 2n$, $h0l{:}l = 2n$, and $0kl{:}k = 2n$ uniquely

(15) Ivanov-Shits, A. K.; Sigaryov, S. E. *Solid State Ionics* **1990**, *40/41*, 76.
(16) Yaroslavtsev, A. B.; Kotov, V. Yu. *Russ. Chem. Bull.* **2002**, 515.

Table 1. Summary of Crystallographic Information for β-$Na_4VO(PO_4)_2$

composition	$Na_4VO(PO_4)_2$
molecular weight	348.84
crystal system	orthorhombic
space group	*Pbca* [61]
a (Å)	16.0068(12)
b (Å)	14.5129(8)
c (Å)	7.0231(5)
volume (Å^3)	1631.5(2)
Z	8
D_{calc}, g·cm^{-3}	2.84
radiation, wavelength (Å)	Mo Kα, 0.71073
θ range for cell determination, no. of reflections	6.6−19.7, 22
μ (cm^{-1})	18.52
color	green
diffractometer	CAD4
data collection mode	$\omega-\theta$
absorption correction	rocking curve
no. of measured reflections	7106
no. of independent reflections ($I \geq 3\sigma$)	2520
θ limits (deg)	2−34
range of *h*, *k*, *l*	$0 \rightarrow h \rightarrow 25$ $0 \rightarrow k \rightarrow 22$ $-11 \rightarrow l \rightarrow 11$
R_{int}	0.029
refinement	on *F*
R/R_w ($I > 3\sigma(I)$)	0.030/0.037
GOF/*w*GOF	0.27/1.97
no. of refined parameters	147
weighting scheme, $(\Delta/\sigma)_{max}$	σ^{-2}, 0.005
$\Delta\rho_{max}$ (e/Å^{-3}) positive/negative	0.81/−0.67

Table 2. Atomic Positions and ADP for β-$Na_4VO(PO_4)_2$

atom	*x*	*y*	*z*	U_{eq}, Å^2
V	0.73383(2)	0.24047(2)	0.71886(4)	0.00652(7)
P(1)	0.37241(3)	0.13897(4)	0.50110(7)	0.00712(11)
P(2)	0.11951(3)	0.10867(3)	0.49850(7)	0.00645(10)
Na(1)	0.88241(5)	0.13792(6)	0.49665(12)	0.01395(23)
Na(2)	0.52511(6)	0.24539(6)	0.25620(12)	0.0155(3)
Na(3)	0.49540(6)	0.99420(7)	0.26969(14)	0.0200(3)
Na(4)	0.72534(7)	0.02388(8)	0.31405(16)	0.0265(3)
O(1)	0.02408(9)	0.10259(11)	0.49137(20)	0.0130(4)
O(2)	0.31677(9)	0.15148(11)	0.68031(19)	0.0120(4)
O(3)	0.31939(9)	0.15883(11)	0.31911(19)	0.0118(4)
O(4)	0.40114(10)	0.03937(11)	0.49981(22)	0.0165(4)
O(5)	0.15989(9)	0.01397(10)	0.49582(21)	0.0131(4)
O(6)	0.14271(9)	0.16382(10)	0.67935(20)	0.0108(4)
O(7)	0.14768(9)	0.16351(10)	0.31980(19)	0.0099(4)
O(8)	0.73829(9)	0.20005(10)	0.50102(18)	0.0092(3)
O(9)	0.44450(10)	0.20703(13)	0.50862(22)	0.0191(4)

give the *Pbca* space group, which was chosen for further refinement. First, the atomic positions for vanadium and phosphorus atoms were refined. Then the coordinates for oxygen and sodium atoms were determined from subsequent difference Fourier synthesis. Final refinement was carried out in anisotropic approximation for thermal parameters. Experimental conditions and crystallographic parameters for $Na_4VO(PO_4)_2$ are listed in Table 1. Atomic positions, isotropic atomic displacement parameters (ADP), and main interatiomic distances in the β-$Na_4VO(PO_4)_2$ structure are given in Tables 2 and 3, respectively.

The crystal structure of $Na_4VO(PO_4)_2$ contains infinite chains of $V^{+4}O_6$ octahedra sharing common apical corners (Figure 4). Neighboring octahedra are additionally linked by two PO_4 tetrahedra resulting in a zigzag chain. Vanadium atoms in the octahedra are shifted from the equatorial plane toward one of two O(8) atoms and, consequently, the V−O(8) distances become nonequivalent: 1.640 and 2.163 Å (Figure 5a). All equatorial V−O bonds are nearly 2 Å. This geometry indicates the formation of one vanadyl bond. These bonds are

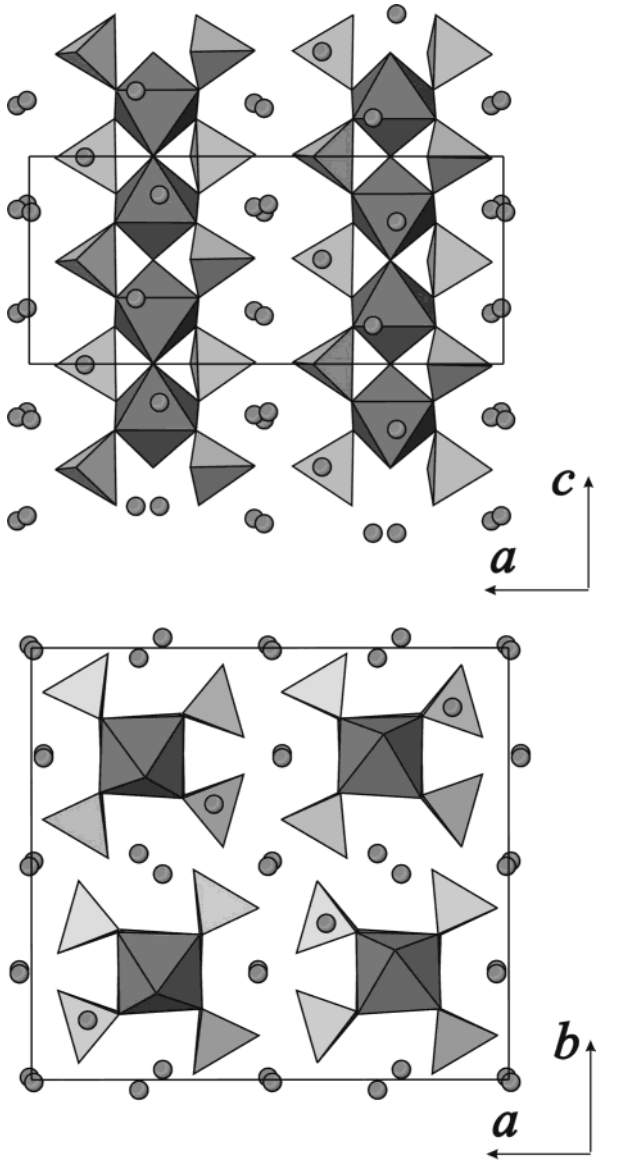

Figure 4. Two projections of the β-$Na_4VO(PO_4)_2$ crystal structure. Circles represent sodium atoms. Vanadium and phosphorus atoms are situated in octahedra and tetrahedra, respectively.

Table 3. Main Interatomic Distances (Å) for β-$Na_4VO(PO_4)_2$

atoms	distance	atoms	distance
V−O(2)	1.9829(15)	Na(2)−O(1)	2.7053(17)
V−O(3)	2.0205(15)	Na(2)−O(1)	2.8303(17)
V−O(6)	1.9687(14)	Na(2)−O(6)	2.3419(17)
V−O(7)	1.9793(14)	Na(2)−O(7)	2.3550(16)
V−O(8)	1.6401(13)	Na(2)−O(9)	2.2622(18)
V−O(8)	2.1627(13)	Na(2)−O(9)	2.2727(18)
P(1)−O(2)	1.5525(14)	Na(3)−O(1)	2.4591(17)
P(1)−O(3)	1.5612(14)	Na(3)−O(1)	2.4272(17)
P(1)−O(4)	1.5169(16)	Na(3)−O(4)	2.3061(18)
P(1)−O(9)	1.5198(17)	Na(3)−O(4)	2.3665(18)
P(2)−O(1)	1.5308(14)	Na(3)−O(5)	3.1452(17)
P(2)−O(5)	1.5189(15)	Na(3)−O(5)	3.2391(17)
P(2)−O(6)	1.5466(15)	Na(3)−O(6)	3.2479(17)
P(2)−O(7)	1.5531(14)	Na(4)−O(2)	2.6330(18)
Na(1)−O(1)	2.3253(16)	Na(4)−O(3)	2.6414(18)
Na(1)−O(2)	2.5079(16)	Na(4)−O(4)	2.579(2)
Na(1)−O(3)	2.4551(16)	Na(4)−O(5)	2.3367(18)
Na(1)−O(5)	2.3066(17)	Na(4)−O(5)	2.4196(18)
Na(1)−O(8)	2.4770(16)	Na(4)−O(7)	2.5565(18)
Na(1)−O(9)	2.460(2)	Na(4)−O(8)	2.8817(17)

directed along the chain as shown in Figure 5b. The calculation of BVS gave a value of +4.1 that confirms

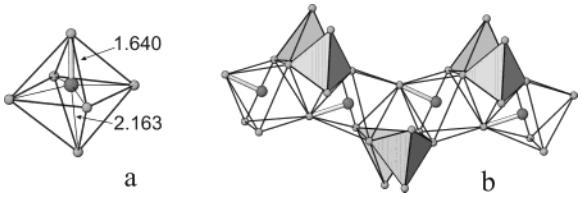

Figure 5. VO_6 octahedron (a) and chain of VO_6 octahedra (b) in the β-$Na_4VO(PO_4)_2$ crystal structure. Large circles represent vanadium atoms and small ones represent oxygen atoms. Vanadyl bond is shown as a thick line.

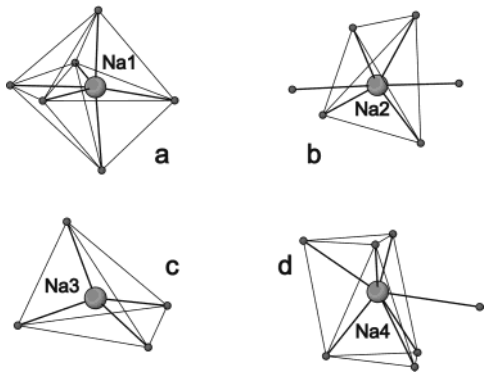

Figure 6. Na polyhedra in the β-$Na_4VO(PO_4)_2$ structure.

the oxidation state for vanadium atoms. All chains in the structure are equivalent. Neighboring chains along the *b*-direction have the same orientation of vanadyl bonds whereas along the *a*-axis these bonds are oriented in an opposite way and related by symmetry. The phosphate tetrahedra are slightly distorted. Sodium atoms are located in an ordered manner in the interstices between the chains. The Na(1) atom coordinates six oxygen atoms, forming a strongly distorted octahedron (Figure 6a). The coordination arrangement of the Na(2) atom may be considered as a bicapped tetrahedron with an average Na(2)−O separation of about 2.3 Å and two additional oxygen atoms are at a larger distance of 2.77 Å (Figure 6b). The coordination polyhedron of the Na(3) atom is a tetrahedron with an average Na(3)−O distance of about 2.4 Å (Figure 6c). The next three neighboring oxygen atoms are separated from Na(3) by more than 3.1 Å. The Na(4) atoms are in the center of a 7-topwood polyhedron, which may be considered as a distorted trigonal antiprism with six Na(4)−O distances of about 2.5 Å and an additional O(8) atom separated by 2.88 Å (Figure 6d).

The crystal structure of β−$Na_4VO(PO_4)_2$ is closely related to that of the high-temperature form of $Na_4TiO(PO_4)_2$. The latter structure also contains isolated infinite chains of corner-shared TiO_6 octahedra linked additionally by tetrahedral phosphate groups. However, the titanium-based compound has a body-centered unit cell (*Ibam*). The main differences between the two structures are related to the position of the transition metal inside the octahedra and to the distribution of the sodium atoms between the chains. The Ti^{4+} cation possesses undistorted octahedral coordination with six almost equal Ti−O bonds (≈1.95 Å). The octahedra in the β-$Na_4VO(PO_4)_2$ structure is only slightly distorted and the average distance of oxygen atoms to the center of the octahedra is also about 1.96 Å. At the same time the V^{4+} cations are shifted toward one of the apical oxygen atoms due to the formation of a short vanadyl bond. This shift results in a reduction of the bond length to 1.64 Å and an increase of the opposite apical distance to 2.163 Å. Furthermore, the sodium atoms in the β-$Na_4VO(PO_4)_2$ structure are completely ordered, in contrast to those in the $Na_4TiO(PO_4)_2$ structure where they are randomly distributed between the chains.

Polymorph modifications of the $Na_4TiO(PO_4)_2$ compound are distinguished by ordering type of sodium atoms, whereas Ti atoms are always situated in the center of the octahedra. In the case of $Na_4VO(PO_4)_2$ an additional opportunity for polymorphism appears due to the presence of a vanadyl bond. So in the β-form both chains (i.e., vanadyl bond direction) and sodium atoms are ordered, resulting in the primitive unit cell. A change of the symmetry from primitive to body-centered at the $\beta \rightarrow \alpha$ transition may occur due to either random orientations of the chains or shift of V atoms to the center of octahedra. Except this, a rearrangement in the Na position may take place. Random orientation of the chains is equivalent to a "disorientation" of the vanadyl bond inside the octahedra and formation of two randomly occupied V-positions with oppositely directed vanadyl bond. Such splitting of the V-position symmetrically corresponds to a shift of the vanadium atom to the center of the octahedron. Therefore, orientation of all chains in the structure becomes equivalent (in terms of vanadyl bond direction) and this should result in the I-centered unit cell which was determined from the electron diffraction study for the α-form. This situation is quite typical for V^{4+} compounds having chains of VO_6 octahedra in their structures.

Electron Microscopy Study. The EDX analysis made on different crystallites was unable to quantify correctly the Na content due to the low *Z*-number, but showed that the V:P ratio remained constant at 1:2 for all measurements.

The $Na_4VO(PO_4)_2$ as-prepared furnace-cooled sample demonstrates transformations under the electron beam, leading to the formation of different superstructure types. Two phases were observed in this $Na_4VO(PO_4)_2$ powder sample, which can be easily distinguished by comparing their [001]* electron diffraction patterns. The different [001]* zones found in this material are shown in Figure 7a−c. However, none of the phases were stable enough to obtain high-resolution real space images, and only the phase corresponding to Figure 7c was stable enough to perform an electron diffraction tilt experiment. However, all crystals on the carbon grid were oriented either close to [001]* or [010]* orientation and the [100]* orientation could not be reached.

Parts (a)−(c) of Figure 7 are successive patterns which can be obtained by either increasing the beam current density or in situ heating. Further, we will call them cases A, B, and C, respectively, to have a compact description. β-$Na_4VO(PO_4)_2$ as determined from XPD agrees with phase B; the C-phase corresponds well with the α-$Na_4VO(PO_4)_2$ from XPD. Figure 7a (case A) can only be achieved when taking great care of exposing the crystallite to only a low dose of irradiation, preventing as much as possible the heating and irradiation of the crystallite; the B(β) phase (Figure 7b) is obtained when slightly increasing the beam current density; the phase is also very unstable and changes into Figure 7c, which is the C(α)-phase. The latter immediately decomposes

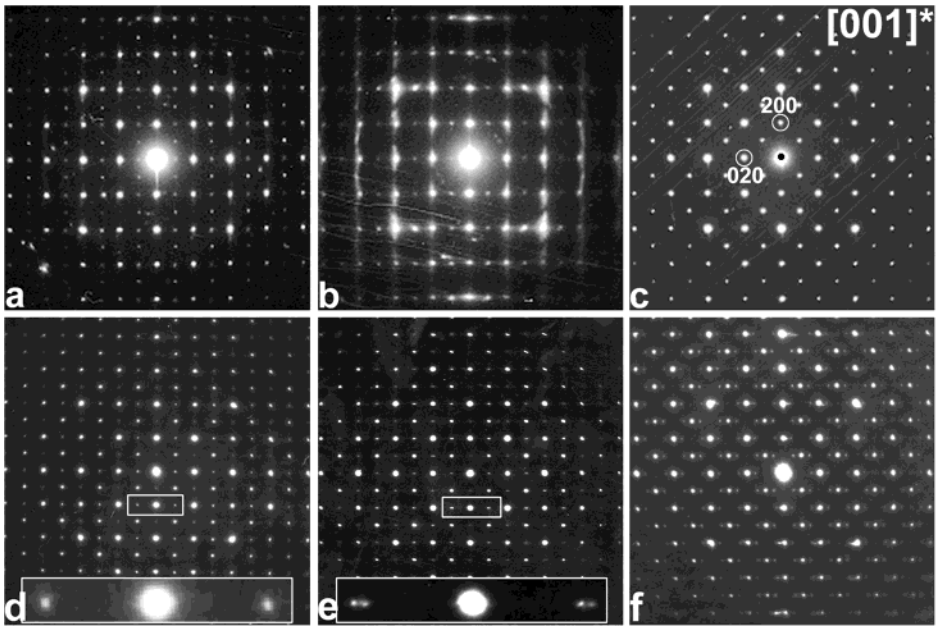

Figure 7. ED patterns of the [001]* zone for $Na_4VO(PO_4)_2$.

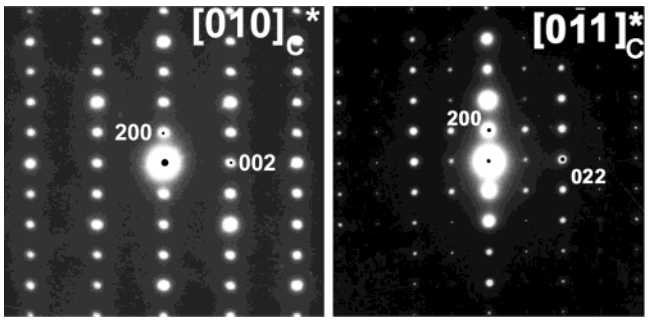

Figure 8. ED patterns of the [010]* and [0$\bar{1}$1]* zones for C (α-$Na_4VO(PO_4)_2$).

under high current density into amorphous material. The [010]* and [0$\bar{1}$1]* ED patterns for C(α) are shown in Figure 8a and b, respectively.

The extinction conditions found for the B(*β*)-phase (Figure 7b) include $hk0{:}h = 2n$ and $0k0{:}k = 2n$. These conditions were obtained from the [001]* zone. For other conditions no conclusion could be made since it was impossible to obtain tilt series from the A and B phases due to their rapid transformation under the beam. Thus, any separate zones found, not belonging to C, could not be conclusively appointed to either A or B. The undubious conditions mentioned above are not very restrictive and leave as extinction symbols a number of possibilities: *Pn.a*, *Pb.a*, or *B*-2_1-, *Bb*- -, *Bb(ac)*-. The second of this row *Pb.a* agrees with the *Pbca* space group found from X-ray single-crystal data.

These transformations can be reproduced in a more controlled way when keeping the material under a low dose beam, as used for A, and applying in situ heating, which was performed in steps of 25 °C, starting from 20 °C. Phase A is then maintained up to approximately 120 °C, after which the B(*β*) phase (Figure 7b) is obtained. This phase is maintained up to approximately 220 °C, after which the C(α)-phase appears; this one does not change anymore until at least 495 °C. We did not study higher temperatures.

As Figure 7a exactly matches an overlapping pattern of both (b) and (c) of Figure 7, it is possible that this diffraction pattern does not indicate a separate phase, but is caused by microdomains of both the B(*β*)-phase and the higher temperature C(α)-phase, with which the latter could be present due to quenching conditions. The influence of the beam could cause the metastable phase to disappear, leaving only the B(*β*)-phase. This suggestion explains a turn on the $\sigma(T)$ plot of about 100 °C. The fact that such presence of domains of the α-phase were not seen on XRD could indicate a very small size of the domains of α.

The extinction conditions found from the tilt series for the C(α) phase include $hkl{:}h + k + l = 2n$, $hk0{:}h + k = 2n$, and $h0l{:}h,l = 2n$ and exclude for $0kl$ the possibility of $k + l = 2n$ as a reflection condition because of the disappearance of the 011 reflection on the [0$\bar{1}$1]* pattern (Figure 8b) when tilting around this direction. This leaves only two possible space groups, *Iba*2 and *Ibam*.

Parts (d)−(f) of Figure 7 represent the main phases (respectively, phases D, E, and F) in as-prepared samples quenched from high temperatures (600−700 °C). Observed phases are more stable under the electron beam than the previous three, but still cannot withstand a high current density as needed for obtaining HREM images. These phases were not seen to transform into any of the above, but immediately went to an amorphous state under higher current density. The difference between Figure 7d and Figure 7a can be clearly seen by the reflections $hk0{:}h = 2n + 1$, $k = 2n$. in Figure 7a found in the furnace-cooled sample these reflections are always absent; in Figure 7d, found in the quenched sample, these reflections are always present.

On XRD patterns of these quenched samples α-$Na_4VO(PO_4)_2$ and/or metastable phase described above and a number of weak unidentified peaks were observed. This can be explained by the correspondence of the basic reflections of these three phases D, E, and F to that of C(α). Within one crystallite several domains were present next to each other containing these phases. When positions were changed on the crystallite, the basic reflections remained the same, and only the

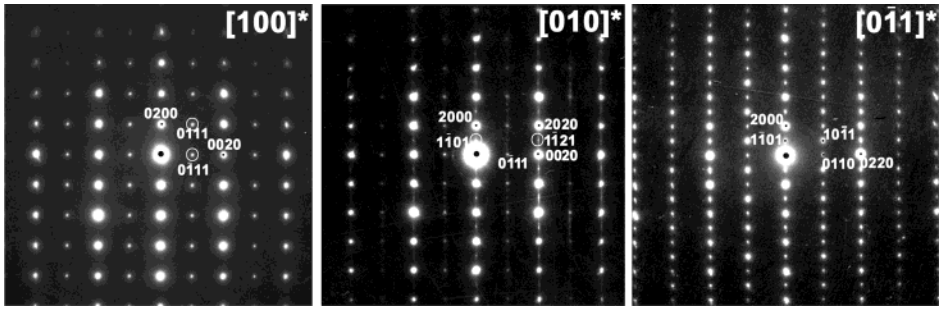

Figure 9. ED patterns of the [100]*, [010]*, and [0$\bar{1}$1]* zones for the D-phase.

modulation reflections changed appearance. Thus, these weaker satellite reflections can be absent on the XRD patterns due to this domain formation and only the constant basic reflections show up, which correspond exactly to those of C(α).

The [100]*, [010]*, and [0$\bar{1}$1]* ED patterns for the D-phase are shown in Figure 9. The correspondence of the basic reflections of D to the reflections of C(α) on Figures 7c and 8 can be clearly observed. The phases E and F (respectively, (e) and (f) of Figure 7) also have the same basic reflections on the [001]* ED pattern as phase C, with additional reflections due to a modulation with modulation vector q along the b-direction. The value of q is $q_E = (0.95 \pm 0.02)b^*$ and $q_F = (0.46 \pm 0.03)b^*$. E and F appear to be incommensurate versions of the same modulation as which causes the commensurate superstructure in D. As such, one description within 3+1-dimensional space can describe all phases C(α), D, E, and F simultaneously. For the D-phase the extinction conditions $hkl0{:}h + k + l = 2n$, $h0l0{:}h = 2n$, $0klm{:}k + m = 2n$ were undoubtedly revealed from at least six sections of the reciprocal space, leading to the 3+1-dimensional space group $Ibam(0\beta0)s00$, $\beta = 1$. Electron diffraction patterns for the forms C(α), D, E, and F of $Na_4VO(PO_4)_2$ (not B(β)) can all be correctly described within this same 3+1-dimensional space group $Ibam(0\beta0)s00$ with β-values of, respectively, 0, 1, 0.95 ± 0.02, and 0.46 ± 0.03. On the [100]* ED pattern for phase D shown in Figure 9, there is an absence of $0k00$ with $k = 2n + 1$, which coincide with the reflections $0k0m$ with $k = 2n$, $m = 2n + 1$, whereas on the [001]* pattern of this same phase these reflections are present. However, they are rightfully absent due to the extinction conditions of, respectively. $hkl0{:}h + k + l = 2n$ and $0klm{:}k + m = 2n$. The presence of these reflections on the [001]* ED pattern is due to double diffraction.

The commensurate space group corresponding to D would be *Pbam*, which is a subgroup of the 3D space group *Ibam* found for the high-temperature C(α)-phase. The space group found from X-ray single-crystal data for β-$Na_4VO(PO_4)_2$ and which agrees also with phase B from electron diffraction is *Pbca*. This change is the result of ordered shifts of vanadium atoms from the center of the octahedra, which leads to an exchange of the mirror plane for a glide one. In the case of a *Pbam* space group vanadium atoms should be situated either in the center of octahedra or statistically occupy positions out of the mirror plane, leading to randomly directed vanadyl bonds. Our electron diffraction study indicates that a formation of such modification with *Pbam* symmetry also takes place. Even more, the ordered β-$Na_4VO(PO_4)_2$ becomes the least stable modification under electron beam irradiation.

Electron diffraction study revealed a presence of several phases with close structure and different types of superstructure. Most of them are not seen on the X-ray patterns. The variety of structural transformations for $Na_4VO(PO_4)_2$ is determined by two main factors: a distribution of sodium atoms between chains with complete or partial ordering (like in the $Na_4TiO(PO_4)_2$ polymorphs) and a presence of the vanadyl bond and different ways of its orientation along the chain. Really, the situation may be even more complicated. This structure can adopt an excess of sodium atoms if an oxidation state of transition metal allows it. For example, the iron-based compound with similar structure $Na_{4.5}FeO_{0.5}F_{0.5}(PO_4)_2$[17] contains Fe^{3+} atoms and excess of sodium ones. Taking into account an ability of vanadium to form mixed valence compounds where $V_V = +4 \pm \delta$, one cannot exclude an existence of other phases compositions differ from $Na_4VO(PO_4)_2$. However, a detailed crystal structure determination for the nonstoichiometric forms is needed to confirm these suggestions.

Magnetic Properties. In both α- and β-modifications, the susceptibility follows nicely between 2 and 400 K a Curie−Weiss law with a very small Curie−Weiss temperature, θ_{CW}. Small deviation from the Curie−Weiss law at high and low temperatures can be accounted for by a small van Fleck contribution and by interactions between the magnetic ions, respectively. The effective moment for both α- and β-phases, 1.65 μ_B, is very close to the value expected for the spin-only value for the V^{4+} ion (1.73 μ_B). In both modifications θ_{CW} is very small, with an absolute value smaller than 2 K, indicating a very weak magnetic interaction between the V-spins. They behave almost like free spins. This very weak magnetic interaction can be understood on the basis of simple arguments for magnetic exchange. From simple crystal field models, one expects the occupied d-orbital of the V^{4+} ion to be perpendicular to the vanadyl bond. This orbital has no overlap with the apical oxygen atom joining two VO_6 octahedra along the chain, leading to a very weak magnetic exchange along the chains. The magnetic exchange between the chains is also expected to be very weak because of the large separation between the chains and the long and complicated exchange paths.

(17) Maximov, B. A.; Klokova, N. E.; Radaev, S. F.; Simonov, V. I. *Kristallografia (Russ.)* **1992**, *37*, 1143.

Conclusions

New vanadyl phosphate $Na_4VO(PO_4)_2$ was synthesized in an evacuated and sealed quartz tube. Reversible phase transition was found at around 200 °C. Crystal structure of low-temperature β-$Na_4VO(PO_4)_2$ contains isolated chains of corner-shared VO_6 octahedra and sodium atoms are orderly situated between the chains. A phase transition is accompanied by a transformation from primitive to I-centered unit cell and a change of ionic conductivity for 1 order of magnitude. Detailed electron diffraction investigation revealed an existence of diverse superstructures resulting from different ordering types in the $Na_4VO(PO_4)_2$ structure.

Acknowledgment. Authors are grateful to NATO (grant PST.CLG.976956), ICDD (Grant-in-Aid APS91-05) for financial support, and M. Kovba and E. Dikarev for help in the synthetic and structural experiment. Part of this work has been performed within the framework of the IAP 5-1 of the Belgian government. E.V.A. is grateful to Russian Science Support Foundation.

Supporting Information Available: Crystallographic information is available for $Na_4VP_2O_9$ (CIF). This material is available free of charge via the Internet at http://pubs.acs.org.

CM0351543